Chemical Engineering Journal 283 (2016) 404–411

Contents lists available at ScienceDirect

Chemical Engineering Journal

journal homepage: www.elsevier.com/locate/cej

Removal of Fe(II) from groundwater via aqueous portlandite carbonation and calcite-solution interactions

Afef Hamdouni [a], German Montes-Hernandez [b,c,*], Mohamed Tlili [a,d], N. Findling [b,c], François Renard [b,c,e], Christine V. Putnis [f,g]

[a] Natural Water Treatment Laboratory, Water Researches and Technologies Center (CERTE), Technopark of Borj-Cedria, PO Box 273, Soliman 8020, Tunisia
[b] CNRS, ISTerre, F-38041 Grenoble, France
[c] Univ. Grenoble Alpes, ISTerre, BP 53, 38041 Grenoble, France
[d] Department of Chemistry, College of Sciences – King Khalid University, 9033 Abha, Saudi Arabia
[e] PGP, Department of Geosciences, Box 1048 Blindern, 0316 Oslo, Norway
[f] Institut für Mineralogie, Universität Münster, Corrensstrasse 24, 48149 Münster, Germany
[g] Nanochemistry Research Institute, Curtin University, PO Box U1987, Perth 6845, Australia

HIGHLIGHTS

- Aqueous $Ca(OH)_2$ carbonation is a powerful method to remove Fe(II) from water.
- Portlandite $Ca(OH)_2$ can also act as softening agent prior to carbonation process.
- Obtained solid-residues (calcite + FeOOH nanoparticles) could find industrial applications.

ARTICLE INFO

Article history:
Received 16 May 2015
Received in revised form 24 July 2015
Accepted 25 July 2015
Available online 29 July 2015

Keywords:
Removal
Carbonation
Oxidation
Iron ferrous
Calcium hydroxide
Calcite

ABSTRACT

Fresh groundwater is sometimes enriched with dissolved ferrous iron (Fe(II)) that restricts its consumption as potable water because it forms colloidal red matter (mainly ferric oxyhydroxides) under oxic conditions at near neutral pH (>6) conditions. As already demonstrated, natural or synthetic calcite material can be used to accelerate the iron oxidation process from Fe(II) to Fe(III), a process that then enhances its precipitation at the calcite-solution interface as confirmed by in situ atomic force microcopy (AFM) observations in this study. The present study mainly reports on a simplified water treatment method to remove ferrous iron (Fe(II)) from water via aqueous carbonation of calcium hydroxide ($Ca(OH)_2$) at ambient temperature (≈20 °C) and moderate CO_2 pressure (10 bar) conditions. In practice, high concentrations of dissolved iron (up to 100 mg/L) can be successfully removed using only 4 g of $Ca(OH)_2$ per liter of Fe-rich solution (close to 100% of efficiency) and a short treatment time is required (<1 h). This method offers various advantages compared with other calcite-based water treatments. For example, other pre-existent dissolved toxic and eutrophic ions such as As, Cu, Cd, Se, P, S, N, etc. can be simultaneously removed from water during the precipitation of calcite and iron oxyhydroxide nanoparticles (<100 nm). Additionally, the dissolution of calcium hydroxide prior to the carbonation process increases the pH (12.4), a process that can act as a softening agent in the water being treated. Finally, the resultant red solid-residue containing mainly calcite and iron oxyhydroxide (FeOOH type) nanoparticles could be reused as pigment or mineral filler powder for industrial applications. This integrated method could be used successfully to remove toxic dissolved ions from water while generating solid residues with industrial uses.

1. Introduction

Iron is often present in groundwaters worldwide and may exist in a soluble form as ferrous iron (Fe^{2+}or Fe $(OH)^+$) or complexed forms as ferric iron (Fe^{3+}) forming colloidal minerals and/or associated with organic matter (e.g. bacterial activity) [1]. Although iron

* Corresponding author at: CNRS, ISTerre, F-38041 Grenoble, France.
E-mail address: German.Montes-Hernandez@ujf-grenoble.fr (G. Montes-Hernandez).

http://dx.doi.org/10.1016/j.cej.2015.07.077
1385-8947/

is an essential nutrient for humans and has beneficial effects on health, its presence in water may cause contaminations, particularly at high concentrations [2–4]. Iron is present in surface groundwater at various concentration levels, usually up to 3–4 mg/L, but in some cases it may reach 15 mg/L [5]. Even at low concentrations, it can influence the taste and esthetic quality of the water. Indeed, the oxygen from air induces its rapid oxidation to form ferric hydroxide or oxyhydroxide precipitates for pH > 6, that can generate toxic derivatives and develop infections such as neoplasia, cardiomyopathy, and arthropathy [6–7].

A large amount of scientific research has been performed on iron treatment, using various techniques such as ion exchange and water softening [8], bioremediation [9], supercritical fluid extraction [10], activated carbon and other filtration materials [11], oxidation with oxidizing agents including chlorine and potassium permanganate [5], by aerated granular filter [12], by adsorption [13], by ash [14] and treatment with limestone [15]. For this latter case, more fundamental studies have investigated the use of natural or synthetic calcite material for iron removal. These studies have clearly demonstrated that calcite treatment has an effective removal potential by catalyzing iron oxidation at calcite-solution interfaces. Moreover, this method is relatively inexpensive compared to other treatment techniques [16–20]. To our knowledge, no attempt has been made to remove Fe(II) from simulated groundwater via mineral aqueous carbonation of portlandite. In contrast, the carbonation process has been applied to produce potable water [21] and also to neutralize the strong alkalinity of lime contained in various solid residues and simultaneously reducing the solubility of some heavy metals and metalloids dissolved in water [22–25]. Aqueous carbonation processes (e.g. controlled calcite precipitation) and calcite-solution interactions can be used to remove several heavy metals and metalloids from polluted water. This process is common in nature and can have direct implications for environmental and technological remediation issues [26–30].

In the present study, two kinds of experiments were performed in order to assess the removal extent and mechanism of Fe(II) from water (1) via direct aqueous carbonation of portlandite or calcite precipitation ($Ca(OH)_{2(s)} + CO_{2(aq)} \rightarrow CaCO_{3(s)} + H_2O$) at room temperature ($T \approx 20$ °C) and moderate pressure (initial $P_{CO_2} = 10$ bar) and (2) by simple calcite-solution interactions at room temperature ($T \approx 20$ °C). The aqueous carbonation of portlandite was recently used to remove oxyanions via a so-called incorporation process, i.e. via anionic substitution of carbonate (CO_3^{-2}) by a given oxyanion [25,30–31]. In the present study, similar carbonation experiments and conventional characterization of interacting solutions (ICP-AES) and solids (FESEM, XRD, SEM-EDX and FTIR) were performed to study the fate of Fe(II) during calcite precipitation. To the best of our knowledge, this is the first laboratory study that investigates removal of iron from water during aqueous carbonation of portlandite. Our goal here is to answer the following practical and fundamental questions. What is the iron removal efficiency compared with simple calcite-solution interactions? What is the reaction mechanism? Is there a competition between iron oxidation and its incorporation in calcite? What is the nature and textural properties of precipitating calcite and iron oxyhydroxide particles?

2. Materials and methods

2.1. Carbonation experiments

Experiments (Table 1) were performed by mixing 0.6 liter of high-purity water with an electrical resistivity of 18.2 MΩ cm, 2 g of commercial portlandite $Ca(OH)_2$ (calcium hydroxide provided by Sigma–Aldrich) with 96% chemical purity (3% $CaCO_3$ and 1% other impurities) and a defined amount of iron (II) from two different iron sources (ferrous sulfate or ferrous chloride supplied by Sigma–Aldrich). These reactants were placed into a titanium reactor (Parr© autoclave with internal volume of 1 L). The solid particles were dispersed by mechanical stirring (400 rpm) for 2 h at ambient temperature (≈20 °C). Then, 10 bar of CO_2 with 99.995% chemical purity (provided by Linde Gas S.A.) was injected into the reactor. This initial pressure of CO_2 corresponds to the total initial pressure in the system. At these temperature and pressure conditions, the vapor phase consists mainly of CO_2 gas in an ideal state. The subsequent pressure drop was monitored visually by a manometer as a function of time until the CO_2 pressure achieved an equilibrium value in this anisobaric gas–liquid–solid system. At the end of the experiment, the reaction cell was depressurized for about 10 min and the solid was recovered, following the procedure of Montes-Hernandez et al. [25]. In order to measure the iron and calcium concentrations, 20 mL of suspension were sampled and filtered through a 0.22 μm pore-size filter at the end of each experiment. All filtered solutions were then acidified with a drop of concentrated HNO_3 solution (3 N) for further ICP-AES measurements.

Table 1
Summary of carbonation and calcite-solution experiments for removal of ferrous iron Fe(II) from water.

Run #	Removal agent	Dose g/L	C_0 (mg/L)	C_{eq}[a] (mg/L)	Removal efficiency (%)	Final pH	Fe(II) source
1	$Ca(OH)_2$	3.3	5	0.0005	99.98	7.87	$FeSO_4$
2	$Ca(OH)_2$	3.3	10	0.0007	99.99	7.67	$FeSO_4$
3	$Ca(OH)_2$	3.3	20	0.02	99.87	7.31	$FeSO_4$
4	$Ca(OH)_2$	3.3	50	0.03	99.85	6.9	$FeSO_4$
5	$Ca(OH)_2$	3.3	100	0.1	99.89	6.46	$FeSO_4$
6	$Ca(OH)_2$	3.3	5	0.0004	99.99	7.04	$FeCl_2$
7	$Ca(OH)_2$	3.3	10	0.009	99.99	6.91	$FeCl_2$
8	$Ca(OH)_2$	3.3	20	0.0007	99.95	6.79	$FeCl_2$
9	$Ca(OH)_2$	3.3	50	0.02	99.95	6.54	$FeCl_2$
10	$Ca(OH)_2$	3.3	100	0.05	99.94	6.38	$FeCl_2$
11	Synthetic calcite	4.5	5	0.0005	99.89	8.44	$FeSO_4$
12	Synthetic calcite	4.5	10	0.001	99.98	8.24	$FeSO_4$
13	Synthetic calcite	4.5	20	0.001	99.99	7.87	$FeSO_4$
14	Synthetic calcite	4.5	50	0.001	99.99	7.56	$FeSO_4$
15	Synthetic calcite	4.5	100	0.001	99.99	7.13	$FeSO_4$
16	Synthetic calcite	4.5	5	0.0008	99.98	8.49	$FeCl_2$
17	Synthetic calcite	4.5	10	0.001	99.98	8.35	$FeCl_2$
18	Synthetic calcite	4.5	20	0.001	99.99	7.94	$FeCl_2$
19	Synthetic calcite	4.5	50	0.0007	99.99	7.51	$FeCl_2$
20	Synthetic calcite	4.5	100	0.0007	99.99	6.91	$FeCl_2$
21	Natural calcite	0.5	10	nd	100	8.35	$FeSO_4$
22	Natural calcite	0.5	30	nd	100	7.99	$FeSO_4$
23	Natural calcite (AFM exp.)	–	50	–	–	–	$FeSO_4$

[a] Measured by ICP-AES (analytical error ≈ 5%); nd: not detected.

2.2. Fe(II)-rich solutions treated with calcite

Complementary experiments (Table 1) were also carried out using high-purity calcite synthesized in house, as reported in

Montes-Hernandez et al. [32]. Thereby 2.7 g of synthesized calcite were placed in the reactor in contact with iron ferrous solutions for comparison with the carbonation process. Moreover, the calcite dose (from 0.5 to 2 g/L) was assessed at ambient P–T conditions using synthetic calcite and natural limestone from Cap Bon region of Tunis. This limestone was chosen because it is abundant in Tunisia where polluted aquifers with iron also exist. For these experiments, a given amount of calcite was added into stabilized Fe(II)-rich solutions in contact with atmospheric air. Here, the pH and redox potential were monitored in situ and various samples (suspensions) were withdrawn as a function of time (typically 0.5, 2, 5, 10, 30, 60 and 120 min). All suspensions were immediately filtered and acidified in order to determine the variation of Ca and Fe concentration during calcite-solution interactions.

2.3. Physicochemical characterization of aqueous solutions

The calcium and iron concentrations were measured by Inductively Coupled Plasma Atomic Emission Spectrometry (ICP-AES Perkin Elmer Optima 3300 DV). The pH was also systematically measured during and at the end of the experiments using a pH meter (MA235). In various calcite-solution interactions experiments the redox potential was monitored by using a portable instrument (portable redox meter HI 98150).

2.4. Characterization of solid products

2.4.1. X-ray diffraction (XRD)

XRD analyses on powders were performed using a Siemens D5000 diffractometer in Bragg–Brentano geometry; equipped with a theta-theta goniometer with a rotating sample holder. The XRD patterns were collected using Cu kα1 ($\lambda_{k\alpha1}$ = 1.5406 Å) and kα2 ($\lambda_{k\alpha2}$ = 1.5444 Å) radiation in the range 2θ = 10–70° with a step size of 0.04° and a counting time of 6 s per step. Calcite was systematically refined by the Rietveld method on XRD patterns using the BGMN software and its associated database [33].

2.4.2. FESEM observations

Selected samples containing pure calcite (white sample) and calcite-iron oxyhydroxides (pink and red samples) were dispersed by ultrasonic treatment in absolute ethanol for 5–10 min. One or two droplets of the suspension were then deposited directly on an aluminum support and coated with platinum for SEM observations. The morphology of crystal faces was observed by using a Zeiss Ultra 55 field emission gun scanning electron microscope (FESEM) with a maximum spatial resolution of approximately 1 nm at 15 kV. Moreover, conventional Energy Dispersive Spectrometry (EDS) chemical analyses were performed to obtain semi-quantitative elemental compositions of the precipitates.

2.4.3. FTIR measurements

The powdered samples were characterized by using infrared spectrometry, with a BRUKER HYPERION 3000 infrared microscope. The infrared beam was focused through a 15× objective and the typical size of the spot on the sample was around 50 × 50 μm^2. The spectral resolution was 4 cm^{-1} and the spectra were recorded in transmission option between 4000 and 500 cm^{-1}. For these measurements, some fine aggregates of calcite-rich samples were manually compressed between two KBr windows in order to deposit a thin film of sample on a KBr window.

2.5. Calcite-Fe(II)–solution interactions by using a flow-through cell in an atomic force microscope (AFM)

One type of experiment was performed where a calcite surface was scanned at room temperature (23 ± 1 °C) using a Bruker Multimode atomic force microscope (AFM) operating in contact mode. The experiment was performed in situ within an O-ring sealed flow-through fluid cell from Digital Instruments (Bruker). The solution was injected with a syringe between each scan, at regular time intervals of approximately 1.5 min, giving an effective flow rate of 22 μL s^{-1}. This flow rate ensures that processes occurring at the mineral surface are reaction-controlled, rather than diffusion controlled [34]. AFM images were collected using a Si_3N_4 tip (Bruker, tip model NP-S20) with spring constants 0.12 and 0.58 N m^{-1}. Images were analyzed using the NanoScope software (Version 5.31r1). At the beginning of the experiment, deionized water was injected over the calcite surface for several minutes, to observe dissolution and flatten the surface. Dissolution of the surface by the formation of etch pits can be observed during this step. Then, a solution containing iron sulfate with 50 ppm Fe(II) was injected across the calcite surface. The initial pH of the solution, measured in the laboratory, was 5.6.

Measurements of step retreat velocity (or etch pit spreading rate) were made from sequential images scanned in the same direction. The retreat velocity during dissolution v_{sum} (nm s^{-1}) given by $v_{sum} = (v_+ + v_-)/2$ (where v_+ and v_- are the retreat velocities of + and − etch pit steps, respectively) was calculated measuring the length increase per unit time between opposite parallel steps in sequential images.

3. Results and discussions

3.1. Iron removal efficiency

Table 1 and Fig. 1 summarize the removal efficiency of iron from water by using fast carbonation (<1 h) of $Ca(OH)_2$ with compressed CO_2 (10 bar) and via simple calcite-solution interactions at room temperature ($T \approx 20$ °C). In all cases, the so-called removal efficiency ((% efficiency = $((C_0 - C_{eq})/C_0) \times 100$); where C_0 is the initial concentration and C_{eq} is the concentration at a given

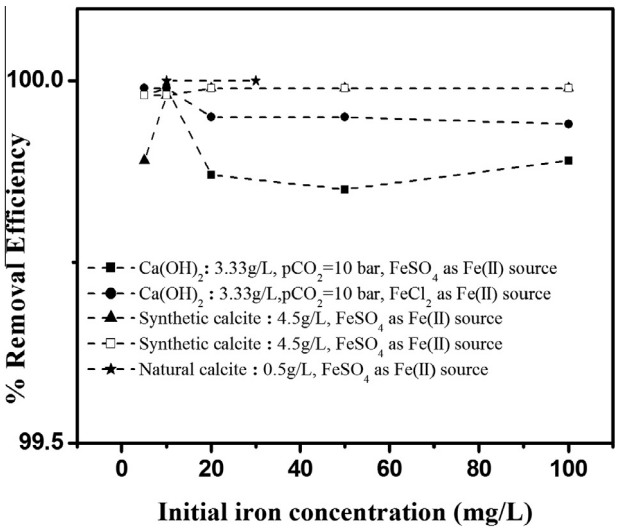

Fig. 1. Removal efficiency of iron by using aqueous carbonation of $Ca(OH)_2$ with compressed CO_2 (initial P_{CO_2} = 10 bar, $T \approx 20$ °C) and by simple calcite-solution interactions at room temperature ($T \approx 20$ °C). Removal efficiency = $((C_0 - C_{eq})/C_0)$ where C_0 is the initial concentration and C_{eq} is the concentration at a given macroscopic equilibrium.

macroscopic equilibrium) is close to 100% for initial concentrations of Fe(II) between 5 and 100 mg/L. In fact, both methods remove successfully the Fe(II) from water and the iron source ($FeSO_4$ or $FeCl_2$) has insignificant impact on the iron oxidation from Fe(II) to Fe(III) and its co-precipitation during calcite precipitation or at calcite-solution interfaces. For example during calcite-Fe-rich solution interactions, the Fig. A-SI shows that the calcite dissolution rate increases with an increase of initial concentration of Fe(II), and is independent of iron source. This means that calcite dissolution in the absence of iron is clearly lower than in the presence of iron (horizontal line in Fig. A-SI). This also indicates that the presence of Fe^{+2} in contact with calcite surfaces promotes calcite dissolution sites during its oxidation and co-precipitation onto calcite surfaces. In other words, calcite particles catalyze the iron oxidation at the calcite-solution interfaces via calcite dissolution, as already described in Mettler et al. [17]. Finally, the removal kinetics is directly dependent on the initial iron concentration, as displayed in Fig. 2a. These results indicate that a dose of 0.5 g of calcite per liter of water is quite sufficient to remove high concentrations of iron (10–30 mg/L) from water within short times (<1 h). The redox potential and pH of the solution also followed a proportional variation with time (see Fig. 2b), i.e. reducing towards oxidant conditions and acidic towards neutral conditions. In summary, high removal efficiency was determined from carbonation experiments or from simple treatment with natural or synthetic calcite.

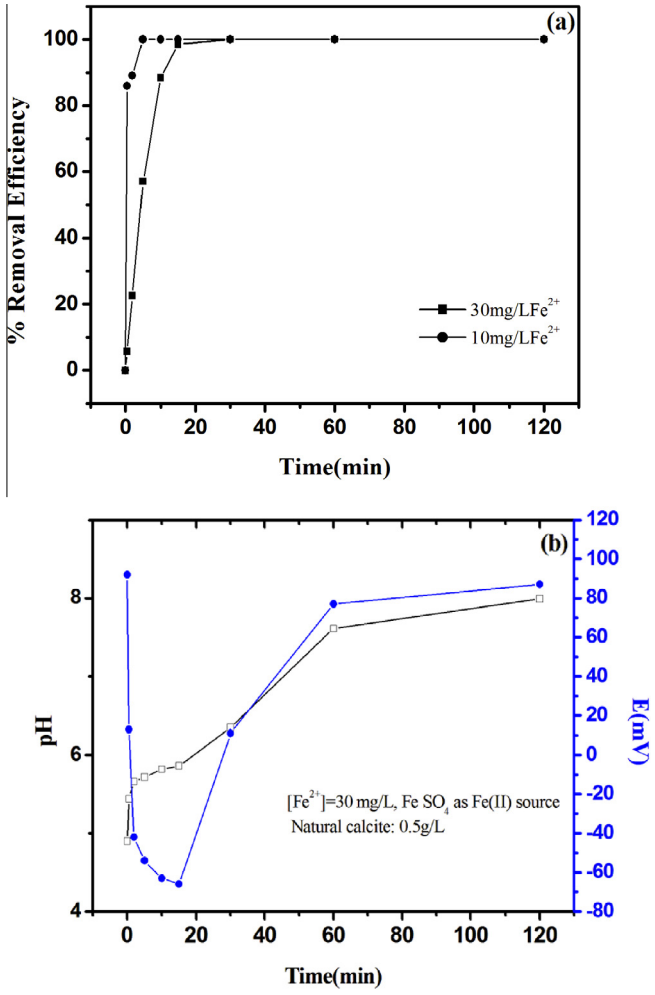

Fig. 2. (a) Kinetic behavior of iron removal efficiency using synthetic calcite as a removal agent. Comparison between two different initial iron concentrations (10 and 30 mg/L). (b) pH and redox potential evolution during calcite-solution interactions.

3.2. Reactions mechanisms

3.2.1. Removal of Fe(II) via aqueous carbonation of portlandite

Aqueous carbonation of portlandite with compressed CO_2 implies various concurrent reactions as already detailed in Montes-Hernandez et al. [25,32,35] and more recently in Fritz et al. [36]. In summary, dissolution of residual portlandite particles $Ca(OH)_2$ is controlled by the absorption-dissociation of carbon dioxide CO_2 until a macroscopic equilibrium is reached. In the present study, small doses of portlandite were used; but, in all cases, the pH increased instantaneously up to 12.4 due to portlandite dissolution:

$$Ca(OH)_{2(s)} \rightarrow Ca^{2+} + 2OH^{-} \text{(dissolution in water)} \quad (1)$$

At this high alkaline pH, the Fe(II) was rapidly oxidized to Fe(III) or complexed with hydroxyl ions:

$$4Fe^{2+} + O_2 + 8OH^{-} + 2H_2O \rightarrow 4Fe(OH)_{3(s)} \text{(oxidation-precipitation process)} \quad (2)$$

$$Fe^{2+} + 2OH^{-} \rightarrow Fe(OH)_{2(\text{s or clusters})} \text{ (complexation and/or precipitation process)} \quad (3)$$

Partial oxidized phases such as magnetite ($FeO{*}Fe_2O_3$ or Fe_3O_4) could also precipitate under high alkaline conditions, but, this mineral, which is stable at ambient conditions, was not observed in the precipitate for our experiments.

The injection of CO_2 in the system implies a fast carbonation reaction and a sudden fall of pH from 12.4 to 5.5 when all portlandite particles are consumed before degassing:

$$CO_{2(g)} \rightarrow CO_{2(aq)} \text{(absorption process)} \quad (4)$$

$$CO_{2(aq)} + H_2O \rightarrow CO_3^{2-} + 2H^{+} \text{ (at high pH, dissociation process)} \quad (5)$$

$$Ca^{2+} + CO_3^{2-} \rightarrow CaCO_{3(s)} \text{(calcite precipitation processes)} \quad (6)$$

As mentioned above, during carbonation the pH changes significantly from 12.4 to 5.5; this can also promote the carbonation of transient phases such as $Fe(OH)_{2(\text{s or clusters})}$ if the initial oxygen content was not sufficient in this closed pressurized system.

$$Fe(OH)_{2(\text{s or clusters})} \rightarrow Fe^{2+} + 2OH^{-} \text{(re-dissolution process)} \quad (7)$$

$$Fe^{2+} + CO_3^{2-} \rightarrow FeCO_{3(s)} \text{(siderite precipitation process)} \quad (8)$$

Conventional characterization of precipitates by DRX, FESEM/EDX and FTIR show the presence of calcite and iron oxyhydroxides (type FeOOH) only. For this reason, we assumed that the ferric iron hydroxide formed by reaction (2), if any, was rapidly transformed to FeOOH during the carbonation process.

$$Fe(OH)_3 \rightarrow FeOOH + H_2O \text{ (probably by dissolution-precipitation process)} \quad (9)$$

Siderite ($FeCO_3$) was not identified in the precipitates. We suggest that siderite fine particles (nanoparticles) if formed could also transform to iron oxyhydroxide (ferrihydrite) during drying via an oxidative reaction process as recently observed in laboratory using siderite nanoparticles (unpublished data). The drying processes imply generally gas–solid reactions where solid state transition

may be the dominant reaction mechanism, however, an interface-coupled dissolution-precipitation mechanism cannot be excluded at low temperature (<100 °C) [37–38].

3.2.2. Removal of Fe(II) via calcite-solution interactions

Mettler et al. [17] have demonstrated that calcite dissolution catalyzes the oxidation of ferrous iron and its co-precipitation as ferric oxyhydroxide at the calcite-solution interfaces. They have mainly used high calcite doses (1–20 g) and low ferrous concentrations (<1 mg/L). Our results reported in Figs. A-SI and B-SI using lower calcite doses (1–4 g/L) and higher ferrous concentrations (until 100 mg/L) confirm macroscopically this hypothesis. In fact, calcite dissolution is directly proportional to the available quantity of iron (see Fig. B-SI). In these simple experiments, a given dose of calcite was directly added into stabilized ferrous solutions in contact with atmospheric air, i.e. acidic pH and reducing conditions were initially constrained by dissolved Fe(II) (see Fig. 2b). The initial acidic pH favors the calcite dissolution as follows:

$$CaCO_3 + H^+ \rightarrow Ca^{2+} + HCO_3^- \text{(calcite dissolution process)} \quad (10)$$

The consumption of protons (H^+) by calcite dissolution progressively increases the pH of the solution (Fig. 2b) and at the same time promotes the Fe^{2+} adsorption and/or complexation with carbonate ions followed by fast iron oxidation in the bulk solution and preferentially at the calcite-solution interfaces:

$$Fe^{2+} + HCO_3^- \rightarrow FeHCO_3^+ \text{ (transient complexation onto calcite and/or in bulk solution)} \quad (11)$$

$$FeHCO_3^+ + 0.5O_2 + H_2O \rightarrow Fe(OH)_{3(s)} + CO_{2(g)} \text{ (oxidation and co-precipitation process)} \quad (12)$$

Similar to carbonation experiments, we hypothesize that the ferric iron hydroxide $Fe(OH)_3$ was rapidly transformed to iron oxyhydroxide (FeOOH type) as described by reaction (9). On the other hand, the CO_2 produced in reaction (12) could be expelled from the solution to the atmosphere (open system) or absorbed-dissociated in the interacting solution depending on pH.

In summary, aqueous carbonation of portlandite and simple treatment with calcite follow different reaction pathways, but, both methods are efficient to remove ferrous iron from water within a short time.

3.2.3. Atomic force microscopy imaging

Direct in situ observations show that in contact with pure water, the (10–14) calcite surface starts dissolving along steps that retreat and through the formation of etch pits with typical rhombohedral shapes (Fig. 3a), as already observed in previous studies (see [39,40] and references therein). Etch pit steps are typically one unit cell (3.5 Å) high. Their retreat velocity was measured to be 2.7 ± 0.3 nm s^{-1}, similar to that observed in previous studies [40].

Interestingly, upon injection of the iron-rich solution, a precipitate formed immediately on the calcite surface and tiny, initially scarce, particles (10 nm large and 10 nm height) grew and covered the surface more or less randomly, and without any observable preferred orientation (Fig. 3b and c). They covered a significant portion of the calcite surface within half an hour. The adhesion of these precipitates was initially weak as they were moved by the AFM tip. These particles nucleated preferentially near step edges and along etch pits, where dissolution would also be faster. No epitaxial growth could be observed. The etch pit retreat rate increased from 2.7 ± 0.3 to 8.4 ± 4 nm s^{-1} during this precipitation, indicating the coupling between dissolution and precipitation. After 30 min the height of these particles was close to 120 nm (Fig. 3d). In summary, these in situ observations confirm spatially and temporally the above reaction mechanism (reactions 10–12).

The precipitate is interpreted to be a lepidocrocite phase because it comes from the dissolution of calcite, the oxidation of iron from Fe(II) to Fe(III) and the precipitation of FeO(OH). This is an example of an interface-coupled dissolution-precipitation process at the mineral-solution surface [38], where the dissolution of calcite increases the pH locally, that then enhances the iron oxydation into Fe(III), allowing for the precipitation of lepidocrocite.

3.3. Nature and textural properties of precipitating particles

For the carbonation experiments, experimental XRD patterns have revealed that calcite is the only crystalline component in all the products (Fig. C-SI). This means that high concentration of iron compounds containing sulfate ($FeSO_4$) or chloride ($FeCl_2$) ions, respectively, have not induced polymorphism because vaterite, aragonite or amorphous calcium carbonate were not detected on the XRD patterns. Rietveld refinement of XRD patterns has revealed small calcite particles only (coherent domain average size <100 nm) in all cases. This indicates also a very weak effect of iron on calcite nucleation and growth at the investigated conditions. These results concerning the particle size of calcite are partially in agreement with FESEM observations. In effect, FESEM observations have revealed that calcite nanoparticles (<100 nm) coexist with sub-micron calcite particles (<1 μm), both forming micron-sized aggregates and agglomerates in the solid material (Fig. D-SI). For this reason, the specific surface area (8–10 m^2/g) is lower than the predicted specific surface area, when assuming isolated cubic or spherical particles [see 35]. Concerning the iron oxyhydroxide, FESEM observations have also revealed the presence of very small nanoparticles (<20 nm) that adhered to calcite crystal faces (Figs. D-SIc and 4) and macroscopically leading to a pink-to-red homogeneous coloration in the solid. However, these very small particles were not detected by XRD analysis, probably due to their small particle size and/or poor crystallinity. This limitation was partially resolved by infrared measurements where transmission infrared spectra have revealed the presence of lepidocrocite (FeO(OH)) as attested by the vibration bands at 3431 cm^{-1} for O–H stretching mode and at 1166 and 1026 cm^{-1}, such peaks being typically assigned to a lepidocrocite mineral phase (Fig. 5) [41]. Unfortunately, the high intensity vibration bands for calcite at 1436, 875 and 709 cm^{-1} obscure the vibration bands for iron oxyhydroxide particles coexisting with calcite in minor proportion. For the calcite-solution interaction experiments, similar infrared signatures concerning iron oxyhydroxide nanoparticles on calcite surfaces were measured indicating as well the presence of lepidocrocite, that is also observed at the nanoscale using AFM imaging (Fig. 3).

3.4. Environmental and technological implications

As mentioned above, a high removal Fe(II) efficiency was determined from carbonation experiments or from simple treatment with natural or synthetic calcite. However, the carbonation method may be triply-efficient because (1) other toxic ions (Se, As, Cd, Cu, Cr, etc.) can be removed during portlandite carbonation by incorporation and/or co-precipitation [25,42] (2) powdered portlandite or calcium hydroxide in water prior to a carbonation process increases the pH to 12.4, which can acts as a softening agent in the water being treated because it favors the simultaneous precipitation of Mg (as $Mg(OH)_2$), Ca (as $CaCO_3$) and other multi-charged cations after carbonation and/or a neutralization process where pH falls within an acceptable range (6–7.5) [43–44] and (3) the resultant red solid-residue containing mainly calcite and iron

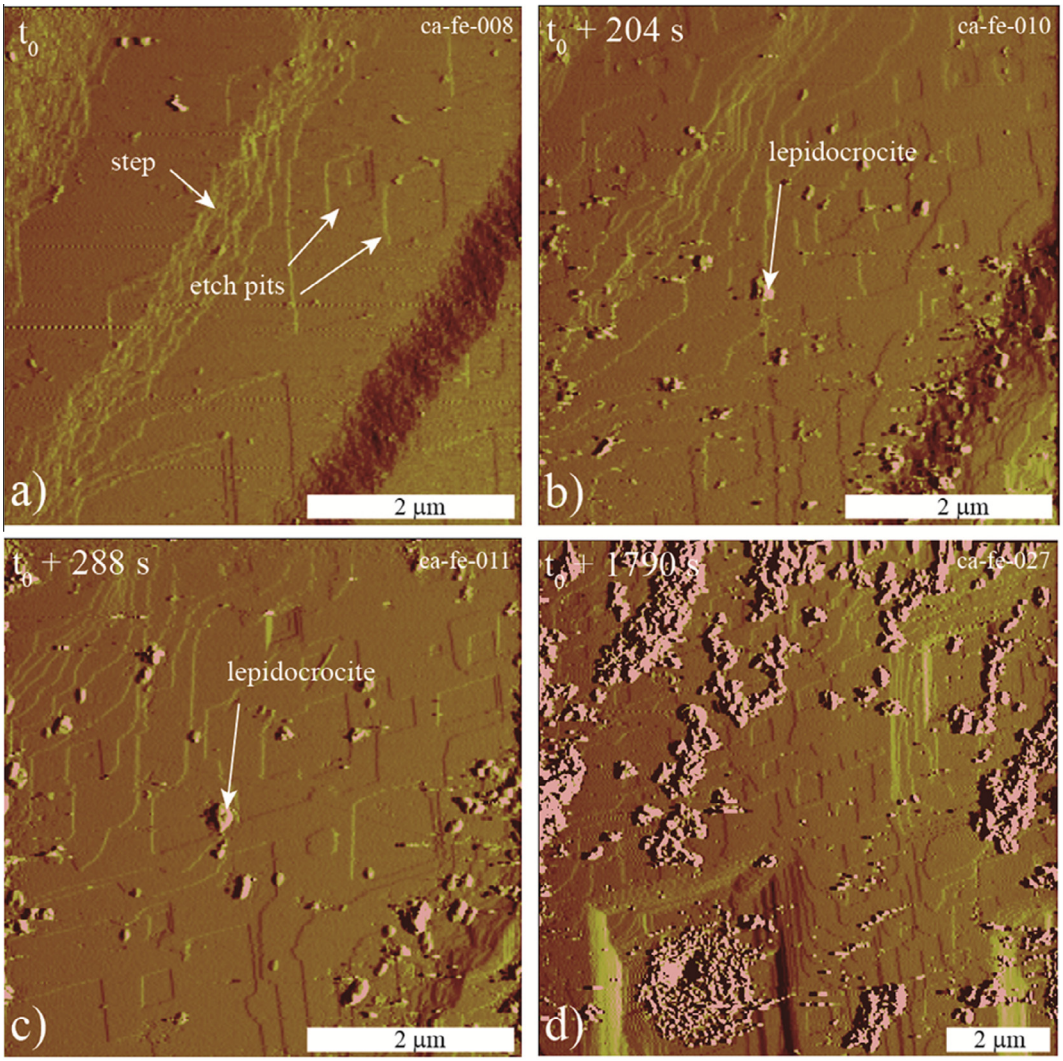

Fig. 3. A time sequence of atomic force microscopy deflection images of a calcite surface during coupled dissolution of calcite and precipitation of lepidocrocite. (a) Dissolution in deionized water, with the presence of etch pits and steps. Each step is 3.5 Å high. (b and c) A solution rich in Fe(II) was injected at time *t* 0 + 60 s, then tiny particles immediately precipitated. (d) After almost half an hour, the surface of calcite is covered by precipitated nano-particles of FeOOH (lepidocrocite).

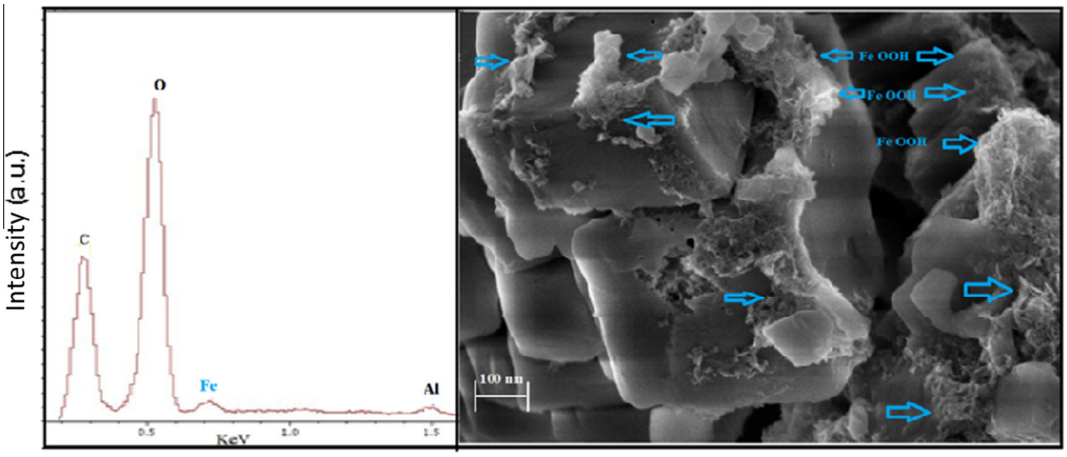

Fig. 4. FESEM-EDS of the precipitate obtained after $Ca(OH)_2$ carbonation reaction in the presence of iron.

oxyhydroxide (FeOOH type) nanoparticles could be reused as a new adsorbent, pigment or mineral filler powder in industrial applications [25,27,45].

The removal efficiency of Fe ions by controlled calcite precipitation is greater when compared to that of other conventional water treatment technologies such as subsurface iron removal (>50%),

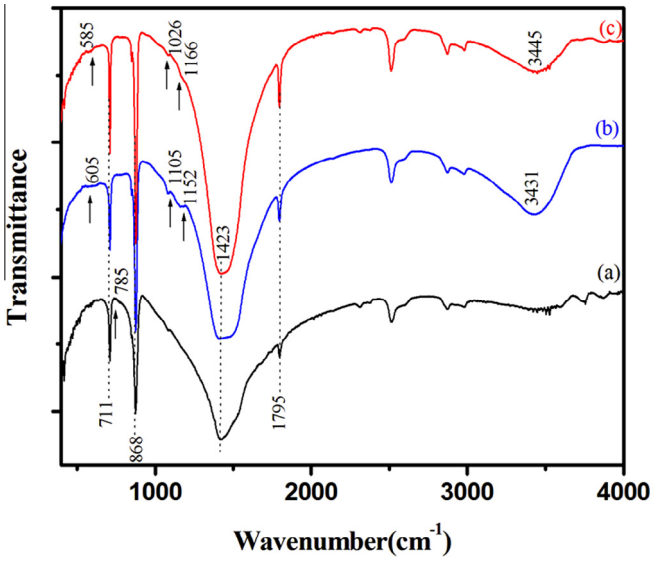

Fig. 5. FTIR spectra of calcite (a) and a mixture of calcite + iron oxyhydroxide formed in the presence of $FeCl_2$ (b) and $FeSO_4$ (c).

bioremediation (70%), aerated granular filter (70%), supercritical fluid extraction (80%), activated carbon and other filtration materials (75–90%), adsorption (84–92%), oxidation/filtration method (80–90%), ion-exchange (90%) and electrocoagulation (95–99%), as shown by Chaturvedi and Dave [46], who summarized all purification methods of water reported in the literature for the removal of iron from groundwater. They claimed that some of these methods are quite effective but they are either cost intensive or suffer from certain limitations when applied in the field. In addition, the proposed carbonation method could be highly economic and ecological, particularly, when the portlandite $Ca(OH)_2$ source comes from alkaline solid waste, because it could allow the simultaneous removal of dissolved toxic and eutrophic ions as well as the mineral sequestration of CO_2 as suggested recently by Montes-Hernandez et al. [25].

Finally, this study reveals also that the Tunisian natural limestone 'RC' may be an effective natural material for the treatment of iron-contaminated groundwater. The use of calcite 'RC' can give a low-cost, simplicity of application and satisfactory efficiency within 2–15 min, for a dose of 0.5 g/L. This is in agreement with studies conducted by Wu et al. [46] and Sdiri et al. [47] who report high efficiency of Tunisian limestone for the removal of heavy metals. Application of calcareous materials (natural or synthetic) to treat ferrous contaminated groundwater has been pointed out by various researchers [15,17–20]. All studies argue that the limestone provides high potential and effectiveness, low cost and ease of use.

4. Conclusion

The present study shows that the aqueous carbonation of portlandite is a powerful method to remove Fe(II) and other heavy metals and metalloids from water. Particularly, high removal efficiencies (close to 100%) were determined using small portlandite doses (2–4 g/L) and only a short treatment time is required (<1 h). Moreover, the obtained solid-residues that contain calcite and iron oxyhydroxide nanoparticles could find industrial applications as pigments and/or mineral fillers in the paper and paint industries. Finally, calcium hydroxide in water prior to a carbonation process can also act as a softening agent in the water being treated because it favors the simultaneous precipitation of Mg (as $Mg(OH)_2$), Ca (as $CaCO_3$) and other multi-charged cations can be also removed after carbonation and/or neutralization processes where pH falls within an acceptable range (6.0–7.5). Finally, aqueous carbonation of portlandite and simple treatment with calcite follow different reaction pathways and both methods are efficient to remove ferrous iron from water within a short time.

Acknowledgements

The authors are grateful to the ANR French research agency (ANR CORO project) and the French National Center for Scientific Research (CNRS) for providing financial support. Funding from Labex OSUG@2020 (Investissement d'avenir-ANR10-LABX56) is acknowledged. D. Tisserand and S. Bureau are thanked for their valuable technical assistance.

Appendix A. Supplementary data

Supplementary data associated with this article can be found, in the online version, at http://dx.doi.org/10.1016/j.cej.2015.07.077.

References

[1] D. Ghosh, H. Solanki, M.K. Purkait, Removal of Fe(II) from tap water by electrocoagulation technique, J. Hazard. Mater. 155 (2008) 135–143.
[2] P. Sarin, V.L. Snoeyink, J. Bebee, K.K. Jim, M.A. Beckett, W.M. Kriven, J.A. Clement, Iron release from corroded iron pipes in drinking water distribution systems: effect of dissolved oxygen, Water Res. 38 (2004) 1259–1269.
[3] D. Van Halem, D.H. Moed, J.Q.J.C. Verberk, G.L. Amy, J.C. van Dijk, Cation exchange during subsurface iron removal, Water Res. 46 (2012) 307–315.
[4] S. Bordoloi, S.K. Nath, R.K. Dutta, Arsenic and iron removal from groundwater by oxidation–coagulation at optimized pH: laboratory and field studies, J. Hazard. Mater. 260 (2013) 618–626.
[5] D. Ellis, C. Bouchard, G. Lantagne, Removal of iron and manganese from groundwater by oxidation and microfiltration, Desalination 130 (2000) 255–264.
[6] E.D. Weinberg, W.A. Geoffrey, The role of iron in infection, Curr. Opin. Infect. Dis. 8 (1995) 164–169.
[7] E.D. Weinberg, Patho-ecological implications of microbial acquisition of host iron, Rev. Med. Microbiol. 9 (1998) 171–178.
[8] K. Vaaramaa, J. Lehto, Removal of metals and anions from drinking water by ion exchange, Desalination 155 (2003) 157–170.
[9] P. Berbenni, A. Pollice, R. Canziani, L. Stabile, F. Nobili, Removal of iron and manganese from hydrocarbon-contaminated groundwaters, Bioresour. Technol. 74 (2000) 109–114.
[10] W.C. Andersen, T.J. Bruno, Application of gas–liquid entraining rotor to supercritical fluid extraction: removal of iron (III) from water, Anal. Chim. Acta 485 (2003) 1–8.
[11] R. Munter, H. Ojaste, J. Sutt, Complexed iron removal from ground water, J. Environ. Eng. 131 (2005) 1014–1020.
[12] C. Bong-Yeon, Iron removal using an aerated granular filter, Process Biochem. 40 (2005) 3314–3320.
[13] S.S. Tahir, N. Rauf, Removal of Fe^{2+} from the waste water of a galvanized pipe manufacturing industry by adsorption onto bentonite clay, J. Environ. Manage. 73 (2004) 285–292.
[14] B. Das, P. Hazarika, G. Saikia, H. Kalita, D.C. Goswami, H.B. Das, S.N. Dube, R.K. Dutta, Removal of iron by groundwater by ash: a systematic study of a traditional method, J. Hazard. Mater. 141 (2007) 834–841.
[15] H.A. Aziz, M.S. Yusoff, M.N. Adlan, N.H. Adnan, S. Alias, Physico-chemical removal of iron from semi-aerobic landfill leachate by limestone filter, Waste Manage. 24 (2004) 353–358.
[16] S. Silvana, A.W. John, Estimating the longevity of limestone drains in treating acid mine drainage containing high concentrations of iron, Appl. Geochem. 22 (2007) 2344–2361.
[17] S. Mettler, M. Wolthers, L. Charlet, U.V. Gunten, Sorption and catalytic oxidation of Fe(II) at the surface of calcite, Geochim. Cosmochim. Acta 73 (2009) 1826–1840.
[18] S. Bordoloi, S.K. Nath, R.K. Dutta, Iron ion removal from groundwater using banana ash, carbonates and bicarbonates of Na and K, and their mixtures, Desalination 281 (2011) 190–198.
[19] S. Bordoloi, S.K. Nath, R.K. Dutta, PH-conditioning for simultaneous removal of arsenic and iron ions from groundwater, Process Saf. Environ. Prot. 316 (2012) 1–10.
[20] W. Yu, S. Saraya, G.T. Timothy, Ferrous iron removal by limestone and crushed concrete in dynamic flow columns, J. Environ. Manage. 124 (2013) 165–171.
[21] J.C. Crittenden, R.R. Trussell, D.W. Hand, Water Treatment: Principles and Design, John Wiley & Sons Inc, New Jersey, 2005.

[22] C.D. Hills, R.E.H. Sweeney, N.R. Buenfeld, Microstructural study of carbonated cement-solidified synthetic heavy metal waste, Waste Manage. 9 (1999) 325–331.
[23] D.J. Lee, T.D. Waite, G. Swarbrick, Effect of calcite on lead rich cementitious solid waste forms, Cem. Concr. Res. 35 (2005) 1027–1037.
[24] Q. Chen, Z. Luo, C. Hills, G. Xue, M. Tyrer, Precipitation of heavy metals from wastewater using simulated flue gas: sequent additions of fly ash, lime and carbon dioxide, Water Res. 43 (2009) 2605–2614.
[25] G. Montes-Hernandez, N. Concha-Lozano, F. Renard, E. Quirico, Removal of oxyanions from synthetic wastewater via carbonation process of calcium hydroxide: applied and fundamental aspects, J. Hazard. Mater. 166 (2009) 788–795.
[26] G. Montes-Hernandez, R. Perez-Lopez, F. Renard, J.M. Nieto, L. Charlet, Mineral sequestration of CO_2 by aqueous carbonation of coal combustion fly-ash, J. Hazard. Mater. 161 (2009) 1347–1354.
[27] G. Montes-Hernandez, F. Renard, R. Chiriac, N. Findling, J. Ghanbaja, F. Toche, Sequential precipitation of a new goethite–calcite nanocomposite and its possible application in the removal of toxic ions from polluted water, Chem. Eng. J. 214 (2013) 139–148.
[28] G. Montes-Hernandez, F. Renard, R. Lafay, Experimental assessment of CO_2-mineral-toxic ion interactions in a simplified freshwater aquifer: Implications for CO_2 leakage from deep geological storage, Environ. Sci. Technol. 47 (2013) 6247–6253.
[29] F. Renard, G. Montes-Hernandez, E. Ruiz-Agudo, C.V. Putnis, Selenium incorporation into calcite and its effect on crystal growth: an atomic force microscopy study, Chem. Geol. 340 (2013) 151–161.
[30] F. Renard, C.V. Putnis, G. Montes-Hernandez, E. Ruiz-Agudo, J. Hovelmann, G. Sarret, Interactions of arsenic with calcite surfaces revealed by in-situ nanoscale imaging, Geochim. Cosmochim. Acta 159 (2015) 61–79.
[31] G. Montes-Hernandez, G. Sarret, R. Hellmann, N. Menguy, D. Testemale, L. Charlet, F. Renard, Nanostructured calcite precipitated under hydrothermal conditions in the presence of organic and inorganic selenium, Chem. Geol. 290 (2011) 109–120.
[32] G. Montes-Hernandez, F. Renard, N. Geoffroy, L. Charlet, J. Pironon, Calcite precipitation from CO_2–H_2O–$Ca(OH)_2$ slurry under high pressure of CO_2, J. Cryst. Growth 308 (2007) 228–236.
[33] T. Taut, R. Kleeberg, J. Bergmann, The new Seifert Rietveld program BGMN and its application to quantitative phase analysis, Mater. Sci. (Bulletin of the Czech and Slovak Crystallographic Association) 5 (1998) 55–64.
[34] E. Ruiz-Agudo, D. Di Tommaso, C.V. Putnis, N.H. De Leeuw, A. Putnis, Interactions between organophosphonate-bearing solutions and (1014) calcite surfaces: an atomic force microscopy and first-principles molecular dynamics study, Cryst. Growth Des. 10 (2010) 3022–3035.
[35] G. Montes-Hernandez, A. Fernandez-Martinez, L. Charlet, D. Tisserand, F. Renard, Textural properties of synthetic calcite produced by hydrothermal carbonation of calcium hydroxide, J. Cryst. Growth 310 (2008) 2946–2953.
[36] B. Fritz, A. Clément, G. Montes-Hernandez, C. Noguera, Calcite formation by hydrothermal carbonation of portlandite: complementary insights from experiment and simulation, Cryst. Eng. Commun. 15 (2013) 3392–3401.
[37] A. Putnis, C.V. Putnis, The mechanism of reequilibration of solids in the presence of a fluid phase, J. Solid State Chem. 180 (2007) 1783–1786.
[38] A. Putnis, Mineral replacement reactions, in: Oelkers E.H., Schott J. (eds) Thermodynamics and kinetics of water–rock interaction. Rev. Min. Geochem. 30 (2009) 87–124.
[39] E. Ruiz-Agudo, M. Kowacz, C.V. Putnis, A. Putnis, The role of background electrolytes on the kinetics and mechanism of calcite dissolution, Geochim. Cosmochim. Acta 74 (2010) 1256–1267.
[40] E. Ruiz-Agudo, C.V. Putnis, Direct observations of mineral-fluid reactions using atomic force microscopy: the specific example of calcite, Mineral. Mag. 76 (2012) 227–253.
[41] M.D. Caki, G.S. Nikoli, L.A. Ili, FTIR spectra of iron(III) complexes with dextran, pullulan and inulin oligomers, Bull. Chem. Technol. Macedonia 21 (2002) 135–146.
[42] B. K. Ambasta, Chemistry for Engineers, Fourth Edition, Laxmi Publications Pvt. Ltd, (2012) 351p.
[43] E. J. Calabrese, Safe drinking water, CRC Press LLC (1989) 240p.
[44] G. Montes-Hernandez, F. Renard, New goethite-calcite composite, its preparation process and its use for the separations of ions (2014) EP2719666 A1.
[45] S. Chaturvedi, P.N. Dave, Removal of iron for safe drinking water, Desalination 303 (2012) 1–11.
[46] X. Wu, W. Hua Pin, D. Nan Sheng, W. Feng, Feasibility study on heavy metal removal from mine water by using geological material, Fresenius Environ. Bull. 12 (2003) 1400–1406.
[47] A. Sdiri, T. Higashi, F. Jamoussi, S. Bouaziz, Effects of impurities on the removal of heavy metals by natural limestones in aqueous systems, J. Environ. Manage. 93 (2012) 245–253.